Altered Translation Elongation Contributes to Key Hallmarks of Aging in Killifish Brain

Domenico Di Fraia[1,15,*], Antonio Marino[1,16,*], Jae Ho Lee[2,17*], Erika Kelmer Sacramento[1], Mario Baumgart[1], Sara Bagnoli[3], Till Balla[4,5], Felix Schalk[1], Stephan Kamrad[6], Rui Guan[6], Cinzia Caterino[1], Chiara Giannuzzi[1,3], Pedro Tomaz da Silva[7,8], Amit Kumar Sahu[1], Hanna Gut[1], Giacomo Siano[3,18], Max Tiessen[1], Eva Terzibasi-Tozzini[3], Eugenio F. Fornasiero[9,10], Julien Gagneur[7,11,12], Christoph Englert[1,13], Kiran R. Patil[6], Clara Correia-Melo[1], Danny D. Nedialkova[4,5], Judith Frydman[2,14#], Alessandro Cellerino[1,3,#], and Alessandro Ori[1,19,#]

[1] Leibniz Institute on Aging - Fritz Lipmann Institute (FLI), Jena, Germany
[2] Department of Biology, Stanford University, Stanford, CA, USA
[3] BIO@SNS, Scuola Normale Superiore, Pisa, Italy
[4] Mechanisms of Protein Biogenesis, Max Planck Institute of Biochemistry, Martinsried, Germany
[5] Department of Bioscience, TUM School of Natural Sciences, Technical University of Munich, Garching, Germany
[6] MRC Toxicology Unit, University of Cambridge, UK
[7] School of Computation, Information and Technology, Technical University of Munich, Garching, Germany
[8] Munich Center for Machine Learning, Munich, Germany
[9] Department of Neuro- and Sensory Physiology, University Medical Center Göttingen, Göttingen, Germany
[10] Department of Life Sciences, University of Trieste, Trieste, Italy.
[11] Computational Health Center, Helmholtz Center Munich, Neuherberg, Germany
[12] Institute of Human Genetics, School of Medicine, Technical University of Munich, Munich, Germany
[13] Institute of Biochemistry and Biophysics, Friedrich Schiller University Jena, Jena, Germany
[14] Glenn Laboratories for the Biology of Aging, Stanford University, Stanford, CA, USA.

Current affiliations:
[15] Department of Biology, University of Rochester, Rochester, NY, USA
[16] Proteomics Research Infrastructure, University of Copenhagen, Copenhagen, Denmark
[17] Department of Biochemistry and Cell Biology, Stony Brook University, Stony Brook, NY, USA
[18] Institute of Neuroscience, Italian National Research Council (CNR), Pisa, Italy
[19] Genentech Inc., South San Francisco, USA

* Equal contribution
# Correspondence should be addressed to: jfrydman@stanford.edu, alessandro.cellerino@leibniz-fli.de or alessandro.ori@leibniz-fli.de

ABSTRACT

Aging is a major risk factor for neurodegeneration and is characterized by diverse cellular and molecular hallmarks. To understand their origin, we studied the effects of aging on the transcriptome, translatome, and proteome in the brain of short-lived killifish. We identified a cascade of events in which aberrant translation pausing led to altered abundance of proteins independently of transcriptional regulation. In particular, aging caused increased ribosome stalling and widespread depletion of proteins enriched in basic amino acids. These findings uncover a potential vulnerable point in the aging brain's biology – the biogenesis of basic DNA- and RNA-binding proteins. This vulnerability may represent a unifying principle that connects various aging hallmarks, encompassing genome integrity, proteostasis and the biosynthesis of macromolecules.

One-Sentence Summary: Increased translation elongation pausing reshapes the aging brain proteome leading to vulnerabilities in the biogenesis of nucleic acid binding proteins.

Keywords: brain, aging, proteome, translation, ribosome, proteasome, mitochondria, killifish, protein aggregation, post-translational modification

Main text

Both aging and neurodegeneration disrupt protein homeostasis, also known as proteostasis, leading to the progressive accumulation of protein aggregates (*1*, *2*). Proteostasis involves mechanisms that regulate the coordination of protein synthesis, degradation, and localization and is essential to ensure an adequate supply of functional proteins. It also prevents the accumulation of misfolded and proteins not assembled in protein complexes that are more susceptible to aggregation.

Age-dependent decline in proteostasis coincides with the emergence of impairment in other aging hallmarks; however, an integrative analysis is needed to establish causality between proteostasis impairment and specific aging hallmarks. This knowledge gap persists, at least partially, because different proteostasis mechanisms have been analyzed separately and in different model systems. Therefore, we comprehensively analyzed proteostasis in the aging brain of the short-lived killifish, *Nothobranchius furzeri*. We focused on the brain because it comprises rarely dividing, largely post-mitotic cells such as neurons, which are more susceptible to proteostasis impairment, a key pathophysiological mechanism in age-related human neurodegenerative disorders. We used killifish as a model organism because of its short lifespan and conserved aging brain hallmarks, such as gliosis, neuroinflammation, senescence, and protein aggregation, as well as spontaneous emergence of neurodegenerative phenotypes (*3*–*8*).

We measured the effects of aging on mRNA and protein abundance, as well as protein post-translational modifications, solubility and subcellular localization, enabling quantification of their relation. We established a protocol for long-term partial inhibition of proteasome activity to investigate if any age-related brain phenotype is induced by this specific dysfunction *in vivo*. Finally, we performed sequencing of ribosome-protected mRNA fragments (Ribo-Seq) (*9*) to assess the contribution of mRNA translation to protein abundance changes. The biosynthesis of specific proteins rich in basic amino acids becomes impaired with age due to aberrant translation elongation and pausing at mRNA stretches encoding lysine and arginine. Such alterations lead to the depletion of subunits of protein complexes involved in DNA repair, transcription, splicing, and protein synthesis, as well as changes in the proteome of mitochondria, all of which correspond to aging hallmarks. Altered translation dynamics provide a mechanistic explanation for the broadly conserved loss of correlation between transcriptome and proteome changes during aging (*6*, *10*–*15*), which has been also linked to neurodegeneration in humans (*16*). Thus, our work reveals how altered biogenesis of a specific subset of proteins with age might further enhance vulnerabilities of the proteostasis network in the aging brain contributing to the exacerbation of other aging hallmarks.

Protein-transcript decoupling in the aging brain

To investigate the disruption of protein homeostasis in aging, we focused on the loss of correlation between changes in gene transcripts (mRNA) and corresponding protein, an evolutionarily conserved phenomenon (*6*, *10*–*15*) here referred to as "decoupling", for which a biological explanation is still lacking. To address the origin of decoupling, we combined RNA sequencing (RNAseq) and mass

spectrometry-based proteomics to quantify age-related changes in corresponding transcripts and protein abundance (Fig. 1 A and B, Fig. S1 A through H). We define "decoupling score" as the difference between protein and transcript changes between young and old samples (*17*). This decoupling score describes discrepancies between transcript and protein changes by identifying subsets of proteins displaying “positive protein-transcript decoupling”, i.e., protein abundance greater than expected from changes of its corresponding transcript, or “negative protein-transcript decoupling”, i.e., protein amounts lower than expected from changes of its corresponding transcript (Fig. 1B and Table S1). The distribution of decoupling scores displayed a median shift towards negative values (Fig. 1C) driven by an overall skew towards decreased abundance of a subset of proteins (Fig. S1D). To assess the reproducibility of this metric, we compared decoupling scores from this study to those obtained by analyzing an independent brain aging dataset (*6*). We detected a significant correlation of decoupling scores between the two datasets (Fig. S1I), despite technical differences in the quantitative proteomics workflows: tandem-mass tags (TMT) based quantification (*6*) compared to label-free Data Independent Acquisition (DIA, this study).

We applied multiple linear regression to interrogate the association between decoupling scores (response variable, N=1188 complete observation) and distinct biophysical properties of transcripts and proteins (N=9 features). This model explained 31% of the decoupling variance (Adjusted R^2 = 0.31, Fig. 1D). We detected estimated protein absolute abundance (see methods, **β**=0.36, P < 2.20E-16) as the parameter with the highest positive correlation with decoupling (Fig. 1E). To include protein half-life as a feature, we used data from the mouse brain (*18*), as such data are not available for killifish. Half-life provided the second highest positive partial correlation (**β**=0.31, P < 2.20E-16, Fig. 1E). On the other hand, the parameters with the highest negative correlation with decoupling were relative transcript abundance (expressed as log2 transcripts per million (TPM) **β**=-0.26, P < 2.20E-16) and proportion of basic amino acids (**β**=-0.13, P = 4.30E-03, Fig. 1 D and E). To dissect the contribution of individual amino acids to decoupling, we calculated a second regression model with protein amino acid composition as the sole predictor variable. There was a significant negative correlation between decoupling and the content of lysine, proline, glutamine, and arginine, whereas the neutral amino acids alanine and phenylalanine, which are enriched in abundant and hydrophobic proteins, positively correlated with decoupling (Fig. 1F).

We investigated whether decoupling affects proteins involved in DNA repair and RNA binding, due to their higher content of basic amino acids relatively to the rest of the proteome (Fig. S1J). Both these groups of proteins showed an age-dependent decrease in protein but no change in transcript abundance (Fig. 1 G and H). On the other hand, myelin components, e.g., myelin basic protein (MBP) and myelin protein P0 (MPZ), and intermediate filament proteins, e.g. glial fibrillary acidic protein (GFAP) and alpha-internecine (INA), characterized by long half-lives and low turnover rates (*Mus musculus* half-life: MBP=~82 days, GFAP=~13 days, INA=~35 days (*18*, *19*)) showed decreased transcript amounts but increased protein abundance with aging (Fig. 1I). We validated a subset of these age-related protein abundance changes using targeted mass spectrometry in an independent set of brain samples (Fig. S1 K through L).

Because the brain of killifish undergoes changes in tissue weight, RNA content (Fig. S2 A through C), and loss of neurons in specific brain regions with age (*5*), we repeated our analyses focussing on a brain region, the optic tectum (Fig. S2D and Table S2), that does not display decreased neuron density with aging (*4*). To account for sex-dependent effects, we used tecta from male and female brains. The optic tectum analyses also revealed age-dependent protein-transcript decoupling of the same protein categories as in the whole brain (Fig. S1 M through N and S2E), independently of the animal's sex

(Fig. S2E). Because previous studies identified organ-specific aging signatures (*20*, *21*), we also investigated age-dependent decoupling in four other killifish organs, liver, muscle, heart, and fin (Fig. S2F and Table S3). Downregulation and negative decoupling of proteins rich in basic amino acids were observed in muscle and fin, but not in the liver and to a lower extent in the heart (Fig. S2 G and H).

Taken together, our data show that aging leads to sex-independent discrepancies between protein and transcript amounts for a subset of proteins in the aging vertebrate brain. Aging similarly affects the transcript-protein balance in other organs, with some inter-organ variation.

Convergence of proteome alterations on ribosomes and respiratory chain complexes

We explored whether decoupling is linked to specific proteome alterations. To do so, we comprehensively characterized age-related changes in protein solubility by implementing a differential detergent extraction protocol (Fig. 2A and S3, and Table S4, (*17*, *22*)), and organelle composition by subcellular fractionation in combination with mass-spectrometry (*23*) (Fig. S4 and Table S4, (*17*)). Additionally, we quantified changes in phosphorylation, ubiquitylation, and acetylation to detect how these post-translational modifications were affected in the aging brain (Fig. S5 and Table S5, (*17*)). We focused on these three classes of post-translational modification because of their roles in neuronal physiology and plasticity (*24–26*), and the availability of protocols for enrichment of such modified peptides. The combined data provided an atlas of changes in organelle proteome composition, protein solubility, and post-translational modifications in the aging brain (Fig. S6, (*17*)), and highlight the impact of aging on a subset of proteins that have been genetically linked to neurodegeneration in humans (Table S6, (*17*) and Fig. S7).

To explore the relation among different types of proteome alteration in the aging brain, we conducted a gene set enrichment analysis on the age-related proteome changes for each of the generated datasets (*17*). By calculating Pearson's correlation coefficient between enrichment scores across datasets, we found positive correlations between protein-transcript decoupling and increased detergent insolubility, a hallmark of protein aggregation (Pearson's $R = 0.28$, $P < 2.20E\text{-}16$), as well as protein phosphorylation (Pearson's $R = 0.26$, $P = 6.67E\text{-}08$), whereas other alterations, for instance, changes in protein ubiquitylation, showed a smaller correlation values (Pearson's $R = 0.11$, $P = 1.23E\text{-}02$, Fig. 2B).

To unbiasedly identify the most prominently affected cellular components in our analysis, we used principal component analysis (PCA) to summarize the normalized enrichment scores (NES, Fig. S8A, (*17*)). We ranked gene ontology (GO) terms by calculating the values of their projections on the first two principal component axes. The highest-ranking terms were related to mitochondrial respiratory chain components, ribosomes, and RNA polymerases (Fig. 2C). These sets of protein complexes were often affected by aging in opposite ways (Fig. 2C). Components of the respiratory chain showed a progressive decrease in their transcripts' abundance and little or no increase in abundance of the corresponding protein (Fig. 2 D and E, Fig. S8B). We validated this small increase using targeted mass spectrometry in an independent set of samples (Fig. S8C). Respiratory chain proteins also showed an overall increase in detergent insolubility with aging, indicative of aggregation (Fig. 2F through G). Importantly, these alterations primarily affected respiratory chain components but not mitochondrial proteins in general (Fig. S8D). To corroborate these findings, we examined our subcellular fractionation data (Fig. S4). This analysis allowed us to identify two key aspects: (i)

changes in the protein composition of aged mitochondria, notably a significant decrease in the relative abundance of mitochondrial ribosomal proteins and an increase in the relative amount of oxidative phosphorylation (Fig. 2H and S8D), and (ii) altered subcellular distribution of specific mitochondrial proteins (Fig. S8 E and F). These analyses support a global remodeling of the mitochondrial proteome during aging.

In contrast to respiratory chain proteins, the abundance of both cytosolic and mitochondrial ribosomal proteins progressively decreased during aging (reaching, on average, a ~25% decrease in old brains) whereas the abundance of their corresponding transcripts increased (Fig. 2 I through J, Fig. S8 G and I). The depletion of selected ribosomal proteins was validated by targeted mass spectrometry and immunoblot (Fig. S8 H through J and S11C). Depletion of ribosomal proteins and negative decoupling was observed during aging in all the organs we analyzed (Fig. S8K). The same pattern was not observed for other genes modulated by the mechanistic target of rapamycin (mTOR) kinase signaling, such as genes carrying a 5' terminal oligopyrimidine (TOP) motif (Fig. S8L), suggesting their decline is independent of major changes of mTOR activity. In the brain, the decreased abundance of ribosomal proteins was accompanied by decreased detergent insolubility (Fig. 2 K and L, Fig. S8 H and I). This alteration might be related to the loss of ribosome stoichiometry and partial assembly or disassembly (*6*). RNA polymerase II components showed similar protein abundance patterns and solubility changes (Fig. S8M).

Together, these analyses show that aging preferentially affected proteins in the mitochondrial respiratory chain, ribosomes, and other DNA- and RNA-binding complexes in different ways. Most of these alterations occurred independently of mRNA changes, thus they may result from post-transcriptional mechanisms.

Impact of proteasome inhibition on the brain proteome

Protein degradation by the ubiquitin-proteasome system regulates protein abundance in organelles and complexes, including ribosomes and mitochondria. Aging is correlated with a decline in proteasome activity (*2*, *6*, *27*). To study the impact of proteasome activity on decoupling, we chronically inhibited its activity to ~50% in the brain of adult killifish over 4 weeks and measured transcriptome and proteome (Fig. 3A and Table S7). GO enrichment analysis revealed adaptive changes to proteasome inhibition such as over-representation of proteasome-related terms (Fig. 3A) and alterations of the proteostasis network (Fig. S9A), including increased abundance of proteasome activators, e.g., the proteasome activator complex subunit 1 (PSME1) also known as PA28α, and key autophagy genes, e.g., *ATG7* (Fig. 3B). Some protein abundance changes induced by proteasome inhibition, e.g., increased amounts of heat shock protein B1 (HSPB1), occurred also in aged killifish brains (Fig. 3B) and were independently confirmed by targeted mass spectrometry (Fig. S9B). Proteasome inhibition led to morphological changes of lysosomes (Fig. 3C), which can be observed also in old brains (Fig. S9C) and is linked to lysosomal storage disorders (*28*), and neurodegenerative diseases (*29*). Similarly to aging, proteasome inhibition reduced mitochondrial content (estimated from the ratio of mitochondrial DNA (mtDNA) to nuclear DNA, Fig. 3D and S9D), and globally decreased mitochondrial protein abundance independent of transcription (Fig. 3D) without altering abundance of master regulators of mitochondrial gene expression (Fig. S9E).

Proteasome inhibition led to an increased abundance of shorter-lived proteins (Fig. S9F) and to decoupling between transcript and protein changes (Fig. S9G and Table S7), consistent with its role in regulating protein turnover post-transcriptionally (*30*). However, when we applied the same linear regression models used for aging, we found proteasome inhibition affected different sets of proteins

with distinct biophysical properties than those exhibiting decoupling due to aging (Fig. S9G). Specifically, proteasome inhibition caused an accumulation of proteins enriched in basic amino acids independently of transcription (Fig. S9G). Indeed, the decoupling scores induced by proteasome inhibition and those observed in aging were negatively correlated (Spearman Rho = -0.25, P < 2.20E-16, Fig. 3E). This included ribosomal proteins (Fig. 3F) and respiratory chain complexes (Fig. 3G). Comparable results were obtained when the same protocol of proteasome inhibition was administered to older fish (29 weeks post hatching) (Fig. S9 H and I, Table S8). Thus, partial proteasome inhibition led to specific alterations in the adult killifish brain, some of which recapitulated aging brain phenotypes. However, decreased proteasome activity does not account for the loss of proteins enriched in basic amino acids observed in the old brains.

Aberrant translation pausing correlates with decreased amounts of proteins enriched in basic amino acids

Our findings show that imbalances in proteostasis during aging do not arise solely from proteasome dysfunction. Other factors, such as differential mRNA translation in old age, could cause the observed discrepancies between transcript and protein abundance. Therefore, we conducted a Ribo-Seq experiment in aging killifish brains (Fig. 4A and Table S9). Tri-nucleotide periodicity and consistent replicates (Fig. S10 A and B) demonstrated the overall quality of the data, whereas comparison between mRNA abundance and ribosome occupancy showed expected correlations (R=0.25, *P* < 2.20E-16, Fig. S10C). Translation efficiency analysis (TE, (*17*)) revealed that TE exhibits a higher correlation with protein changes (R=0.32, P < 2.20E-16, Fig. 4B) than transcript changes (R=0.23, P < 2.20E-16), consistent with observations in mammals (*31*). For instance, shifts in TE led to consistent changes in protein abundance for certain protein complexes, such as the Complex IV of the respiratory chain and the 26S proteasome (Fig. 4 C andD and S10D). However, TE did not explain the decreased proteins of ribosomes, RNA polymerase II, and other nucleic-acid binding proteins linked to DNA repair during aging (Fig. 4C and D and S10D). This analysis excludes TE as the cause of the decreased abundance of these proteins in aging brains.

We drew inspiration from studies on aged nematodes and yeasts, which exhibit age-related impaired translation elongation and increased ribosome pausing (*32*). We searched our Ribo-Seq data for signatures of translation pausing (*17*), revealing an overall increase in site-specific pausing in the aging brain (Fig. 4E and Table S9). Disome analysis confirmed an increase in ribosome collisions in the aged brain (Fig. 4F). Age-linked increased pausing was also observed in the liver, albeit to a lower extent than in the brain (Fig. S11A).

Elongation stalling leads to ubiquitination of specific subunits of the 40S ribosome by the ribosome quality control (RQC) machinery (*33–35*). Indeed, anisomycin-induced ribosome stalling in killifish cells induced a characteristic higher molecular weight ubiquitylated band in immunoblots of 40S subunit RPS3 (Fig. S11B), commonly associated with ribosome stalling (*33–35*). Analysis of aged brains showed similarly increased ubiquitination in RPS3 (Fig. S11C), even though ubiquitination of most ribosomal proteins decreased with age (Fig. S11D). Additionally, we noted an aging-dependent increase of ATF3 mRNA (Fig. S11E), a transcription factor whose abundance increases upon sensing of ribosome collisions as part of the Ribosome Stress Response (*36*, *37*). As observed in aged yeast and nematodes, we also observed a decrease in the levels of a subset of proteins involved in RQC (Fig. S11F). This RQC reduction may exacerbate ribosome collisions and stalling as age progresses, potentially slowing stalled mRNA degradation and causing their accumulation in aging cells.

We investigated the impact of translation pausing on cellular proteostasis. We observed a positive association between transcripts subject to increased translation pausing with age and increased age-dependent detergent insolubility of their encoded polypeptide, indicative of aggregation (Fig. 4G). As these alterations affected key proteostasis network components such as the proteasome (Fig. S11G), the increase in elongation pausing and associated aggregation may create a vicious cycle of proteostasis collapse. Stretches enriched in codons for basic residues (arginine and lysine), as well as glycine, were enriched at sites of aging-linked elongation pausing (Fig. 4H) and disome forming sites (Fig. S11H). Our decoupling model linked enrichment in these same residues (arginine and lysine) to reduced protein abundance with age (Fig. 1F). Furthermore, we found a small but statistically significant correlation between increased elongation pausing and protein-transcript decoupling (Fig. 4I, R=-0.17, P < 2.20E-16), which explained changes in ribosomal and RNA-binding proteins, where protein decline did not follow transcript changes. In contrast, pausing in transcripts encoding components of the respiratory chain did not deviate from the overall pausing distribution (Fig. 4I).

Changes in translation and pausing affect mRNA half-life (*38–40*). Therefore, we investigated the association between translation pausing and computationally estimated mRNA half-life in our RNA-Seq data (*17*, *41*). Transcripts encoding ribosomal proteins and RNA-binding proteins show an increased half-life in old brains compared to the rest of the transcriptome (Fig. 4J). Thus alterations in translation might influence other aspects of the aging brain transcriptome, such as the half-life of specific mRNAs. These analyses show that increased ribosome occupancy does not necessarily result in enhanced protein synthesis in the aging brain. Our comprehensive analysis of transcription, translation, protein abundance, and protein solubility in the aging brain indicates that translation dysfunction, and specifically aberrant elongation pausing, may underlie the decreased abundance of ribosomal proteins and other nucleic-acid-binding proteins in the aging brain.

Effect of aging on the abundance of amino acids and tRNA charging

To understand how age-related translation pausing occurs, we examined how metabolic changes affect abundance of certain amino acids and whether aging influences the amounts and charging of tRNAs, as these factors could cause codon-specific alterations in translation supply for the ribosomes. We measured the abundance of amino acids, total and charged tRNA pools, and the protein levels of tRNA synthetases (Fig. 5A, Tables S10 and S11). Amounts of multiple amino acids were altered in the aged brains, with arginine decreased by one half (Fig. 5 B and C, Fig. S12A). tRNA amounts correlated with weighted codon usage in both young and old fish brains (Fig. 5D) and their total abundance was not affected by aging (Fig. 5E). Of note, tRNA charging state was globally decreased with aging across all the tRNAs irrespectively of the amino acid they carry (Fig. 5F). Abundance of multiple tRNA synthetases, including arginine tRNA synthetase (RARS), was decreased in the old brains (Fig. S12B). Given that the changed amounts of charged tRNAs with ageing do not mirror the changes in amino acid pools, decreased abundance of tRNA synthetases might explain decreased tRNA charging in old brains. We investigated the relation between changes in tRNA charging and the age-related increase in translation pausing. This analysis revealed that changes in tRNA charging were not correlated with increased translation pausing (R=-0.13, P=0.3, Fig. 5H), even though some codons clearly showed both increased pausing and decreased charging of their corresponding tRNA, e.g., Arg-ACG (Fig. 5 G and H). Together, these data show that aging affects the abundance of amino acids and tRNA charging in the brain. Decreased tRNA charge may contribute to, but does not fully explain, the increased ribosome pausing observed in old brains.

A possible model for protein biosynthesis in the aging brain

We observed alterations in protein synthesis in old brains, leading to decreased abundance of ribosomal proteins, among others. The reduced abundance of ribosomal proteins may reflect lower numbers of ribosomes in old brains. To confirm that aging decreases the amounts of fully assembled and translating ribosomes, we isolated polysome-containing fractions from the brains of young and old fish on sucrose gradients and quantified ribosomal proteins by mass spectrometry. We confirmed a reduced abundance of ribosomal proteins in polysome fractions relative to that of monosomes (80S) in old brains (Fig. S13).

Altered ribosome concentration can directly impact the translation of specific mRNAs, as observed in a group of inherited diseases collectively referred to as 'ribosomopathies' (*42*, *43*). Protein output of specific mRNAs has been predicted to be influenced by ribosome availability depending on transcript-specific translation initiation rate k_i (where k_i refers to the affinity of specific mRNA sequences to bind ribosomes) (*17*, *42*, *43*). Under these assumptions, a decrease in ribosome concentration might, for example, increase protein synthesis from transcripts with a high translation initiation rate by lowering the total number of ribosomes on them, relieving trafficking and pausing events (Fig. 6A). To test this hypothesis in the context of an aging brain, we estimated k_i from killifish 5'-UTR sequences based on experimental data (*44*) and modeled the estimated synthesis rate as described in (*17*, *42*, *43*) (Fig. 6A, Table S12). A subset of killifish transcripts had increased predicted synthesis rates as a function of decreased ribosome concentration (orange cluster in Fig. 6A and Table S12). In our experimental data, we selected a specific set of proteins showing decreased translation pausing and increased protein abundance in our decoupling model (60 proteins, bottom right quadrant in Fig. 4I). We estimated their predicted synthesis rates as a function of ribosome concentration. Consistent with the experimental data, the relative synthesis of this subset of proteins was predicted to increase following a reduction of ribosome concentration (Fig. 6B). Approximately one-third of these proteins were mitochondrial (including 7 components of the respiratory chain), and another prominent fraction belonged to proteins related to neuron projections (Fig. 6B). The absence of ribosomal proteins in this subset, despite their high k_i value, indicates distinct translation dynamics for these proteins possibly resulting from their increased elongation pausing during aging. We propose that the decreased abundance of ribosomal proteins in the aged brain, possibly triggered by aberrant pausing events, might reduce the availability of translating ribosomes and, thereby, alter abundance of a subset of the proteome independently of transcript abundance (Fig. 6C).

Discussion

Our study offers insight into how distinct proteostasis mechanisms reshape the vertebrate brain proteome during aging. We show proteome changes in aging brains, encompassing protein synthesis, solubility, post-translational modifications, subcellular localization, and organelle composition. Among these, we show that abundance of ribosomal subunits and DNA or RNA binding proteins decrease independently of mRNA abundance. We propose that translation alterations, including elongation pausing at sequences enriched in basic residues, are central drivers of these changes, leading to discrepancies between mRNA concentrations, ribosome occupancy, and protein synthesis. Supporting an age-dependent increase in elongation pausing, we identified changes in protein ubiquitylation in ribosomal proteins that have been associated with ribosome collision induced by different types of translation or proteotoxic stress (*34*, *35*). Consistent with these findings, we also

observed an age-related increase in the mRNA abundance of the transcription factor ATF3, indicative of activation of the ribosomal stress response pathway (*36*, *37*).

At least two key implications emerge from our findings. First, aging leads to decreased abundance of protein complexes containing polybasic stretches, including ribosomes, spliceosomes, RNA and DNA polymerases, and those functioning in DNA repair. This phenomenon, which correlates with the content of basic amino acids in their protein sequences and consequently with their likelihood to be affected by ribosome stalling (*45*) (Fig. 4H, Fig. S1J and Fig. S11H), may impact on multiple steps of the gene expression process and could mechanistically place proteostasis impairment upstream of other canonical aging hallmarks, such as DNA damage, epigenetic alterations (*46*), aberrant splicing (*47*) and reduced RNA polymerase activity (*48*) (Fig. 6C).

A second implication is that aging leads to altered mitochondrial composition. These changes encompass a decrease in abundance of mitochondrial ribosomal proteins and possibly mitochondrial translation whereas respiratory chain components remain stable or increase in abundance. This is consistent with broader observations of aging-induced mitochondrial changes (*49*, *50*). These findings based on bulk tissue measurements were corroborated by more direct analysis of the composition of mitochondria from subcellular fractions and by other age-dependent alterations of mitochondrial proteins, e.g., in detergent insolubility. Decreased mtDNA content appears to be induced by decreased proteasome activity, showcasing the convergence of different proteostasis mechanisms affecting critical cellular structures during aging.

The mechanisms leading to increased translation pausing remain unclear. Our analysis indicates enhanced age-dependent pausing at polybasic enriched sequences, which are known to slow down translation (*45*, *51–53*). These sequences might represent the first ones to reveal impaired elongation when the availability of key factors required for protein synthesis become more scarce in aged cells. In old brains, we found alterations in amino acid abundances, tRNA charging as well as the levels of key RQC factors that might contribute, at least in part, to the observed increase in elongation pausing. Additional mechanisms contributing to increased translational pausing could result from the decreased abundance of ATP observed in old tissues (*54–57*). Decreased energy might alter the decoding kinetics for specific non-optimal codons, such as those encoding basic amino acids (*58*, *59*), leading to a decreased synthesis rate for these proteins. It remains unclear whether these signatures are a cause or consequence of increased ribosome pausing in the aging brain.

Decoupling in aging manifests as a decrease in protein abundance of ribosomal proteins together with a progressive increase in transcript amounts, not only in the brain but also in the fin, heart, liver, and muscle. These findings are consistent with observations from various species. An age-dependent increase of transcripts encoding for ribosomal proteins was observed by single-cell RNAseq in multiple cell types of the murine brain (*60*). Accordingly, increased transcripts encoding for ribosomal proteins were among the most consistent transcriptional signatures of longevity shared across multiple tissues and mammalian species (*61*). Our results indicate that this increase might not result from increased transcription but rather from increased mRNA stability. Decreased abundance of ribosomal proteins with age has been described in multiple organs in mice (*62*), as well as in nematodes (*63*), and the protein half-life of ribosomes is affected by aging in the mouse brain (*64*). These data identify reduced content of ribosomal proteins as a hallmark of aging in vertebrates. We found decreased abundance of DNA and RNA binding proteins occurring independently of mRNA abundance, i.e. decoupling, in other killifish organs including fin and muscle, but not in the liver. Aged livers had

less translation pausing and decrease of basic protein concentration than did the brain. This points to tissue-specific differences in protein synthesis regulation during aging, consistent with observations in rodents (*31*). In mice, different organs age at distinct rates (*20*, *65*). Relevant to our findings, the brain is especially sensitive to aging, with an overwhelming number of late-onset neurodegenerative diseases affecting the brain.

The proteome composition in the aging brain may be influenced by additional processes. For instance, age-dependent impairment of protein degradation by the autophagy-lysosome system can lead to the accumulation of specific proteins (*66*), as has been shown for myelin basic protein (MBP) in mouse microglia (*67*). Consistently, we observed accumulation of MBP and other myelin proteins independently of mRNA changes. A similar impairment of protein clearance might also occur in the aging killifish brain. Stalling of RNA polymerase II occurs with aging, thereby skewing the transcription output in a gene-length dependent manner (*48*), consistent with a systemic loss of long transcripts observed in multiple aging tissues and species (*68*). A reduction in the abundance of specific transcripts could increase transcriptional noise, lead to an imbalance in the stoichiometry of protein complexes, overwhelming proteostasis and altering the relationship between mRNA and protein abundance, especially for long-lived proteins. Aging may also affect post-transcriptional RNA modification (epitranscriptomics), which influences RNA stability and translation in different contexts, including aging (*69*, *70*). It is conceivable that mRNA modifications might contribute to protein-transcript decoupling. Finally, we have identified multiple alterations of protein post-translational modification, most notably phosphorylation. Some of these have been linked to protein aggregation in human neurodegenerative disorders, e.g., hyperphosphorylation of MAPT (*17*).

Our work contributes to advancing our understanding of the relationship between aging and the risk of neurodegenerative diseases. We provide a resource (accessible at https://genome.leibniz-fli.de/shiny/orilab/notho-brain-atlas/) of proteome alterations in the aging killifish brain and show that multiple proteins and signaling pathways associated with neurodegeneration in humans become perturbed in various ways during physiological aging in killifish ((*17*) and Fig. S6, S7). Such alterations might underlie convergent mechanisms between aging and mutations that increase the risk of neurodegeneration in old individuals. Translation pausing might represent one of such converging pathophysiological mechanisms, given that ribosome stalling is correlated with proteostasis perturbation in various neurodegenerative diseases (57–60).

Acknowledgments

The authors gratefully acknowledge support from the FLI Core Facilities Proteomics, Sequencing, Life Science Computing and the Fish Facility, as well as the Stanford Genomics Facility and the NGS Facility in the Department of Totipotency at the MPI of Biochemistry and Cinzia Caterino for assistance in sample preparation and animal experiments.

Funding:
A.O. is supported by the German Research Council (Deutsche Forschungsgemeinschaft, DFG) via the Research Training Group ProMoAge (GRK 2155), the Else Kröner Fresenius Stiftung (award number: 2019_A79), the Fritz-Thyssen Foundation (award number: 10.20.1.022MN), the Chan Zuckerberg Initiative Neurodegeneration Challenge Network (award numbers: 2020-221617, 2021-230967 and 2022-250618), and the NCL Stiftung. J.H.L. acknowledges support by the National Institute on Aging

of the National Institutes of Health under Award Number T32 AG000266. J.F. is supported by NIH grants GM056433 and AG054407. A.C. is supported by the German Research Council (Deutsche Forschungsgemeinschaft, DFG, award numbers CE 257/9-1 and CE 257/9-2), by Next Generation EU (PNRR), "Tuscany Health Ecosystem", THE project code ECS 00000017 and the Italian Ministry of University and Research (MIUR) with the program “Joined research for Special Status School”, PRO3. E.F.F. is supported by a CZI Collaborative Pairs Pilot Project Award (Cycle 2; Phase 1) and acknowledges the support of the SFB1286, Göttingen, Germany. The Max Planck Society supports D.D.N., the European Research Council under the European Union’s Horizon 2020 Research and Innovation Programme (ERC Starting Grant number 803825-TransTempoFold) and the German Research Council (Deutsche Forschungsgemeinschaft, DFG, award number NE 2315/2-1). The content is solely the responsibility of the author(s) and does not necessarily represent the official views of the National Institutes of Health. The FLI is a member of the Leibniz Association and is financially supported by the Federal Government of Germany and the State of Thuringia. K.R.P, S.K. and R.G. acknowledge support from UK Medical Research Council (project no. MC_UU_00025/11).

Author contributions:
Conceptualization: D.D.F., A.M., J.F., A.C., A.O. Data curation: D.D.F., A.M., J.H.L., A.K.S., M.T., E.F.F., C.G. Investigation: D.D.F., A.M., J.H.L., E.K.S., M.B., S.B., T.B., H.G., S.K., K.R.P., F.S. Methodology: D.D.F., A.M., J.H.L., E.K.S., M.B., S.B., F.S. Project administration: J.F., A.O., A.C. Data analysis: D.D.F., A.M., J.H.L., F.S., P.S., G.S., E.F.F., D.D.N., C.G., S.K., R.G. Supervision: E.T.T., J.G., C.E., C.C-M., D.D.N., J.F., A.C., A.O., K.R.P. Visualization: D.D.F., A.M., J.H.L., S.B. Writing – original draft: D.D.F., A.M., A.O. Writing – review & editing: J.H.L., E.K.S., M.B., S.B., P.S., A.K.S., G.S., J.F., A.C., E.F.F.

Competing interests:
The authors declare no competing interests.

Data and materials availability:
All data generated in the study have been deposited in public databases. Please refer to the Data availability section for accession numbers for different datasets.

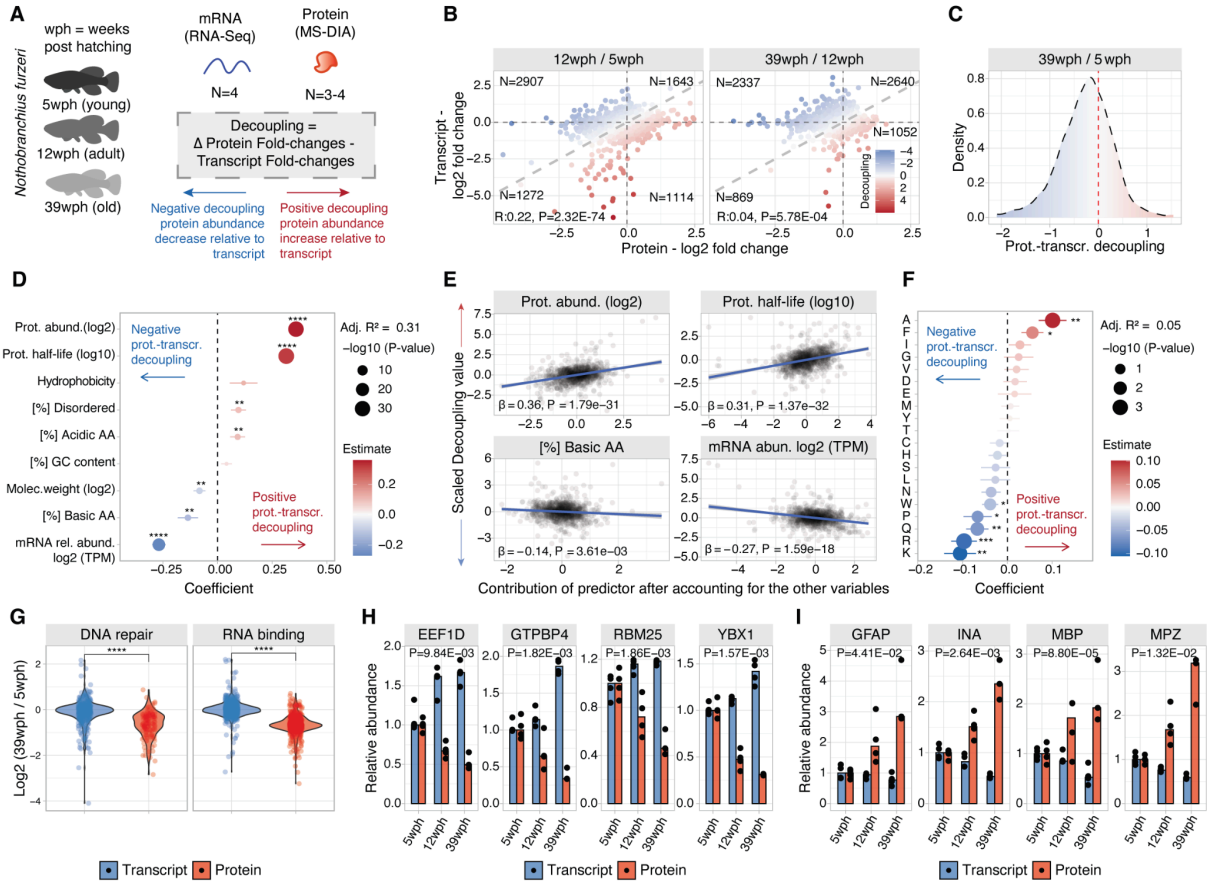

Figure 1: Changes of protein and mRNA abundance are decoupled in the aging brain. A) Characterization of protein-transcript decoupling in the aging brain of killifish, age is reported as weeks post hatching (wph). Positive decoupling values indicate increased protein abundance relative to transcripts, while negative decoupling indicates decreased protein abundance compared to transcripts. B) Scatterplot comparing protein and transcript fold changes in the aging brain. Color represents decoupling score, red – increased protein abundance relative to the transcript, and blue – decreased protein abundance compared to the transcript. Grey dashed lines indicate equal changes. Pearson's R correlation coefficient was calculated between log2 transformed protein and transcript changes. C) Density distribution of decoupling scores for young vs. old comparison. Red: positive decoupling, Blue: negative decoupling. D) Multiple linear regression analysis of decoupling scores based on transcript and protein features. F-test. E) Added variable plot between features and decoupling scores. Protein half-life data were obtained from a mouse brain dataset (*16*) since no data of comparable depth is available for killifish. F) Multiple linear regression analysis of decoupling scores based on protein amino acid composition. F-test. G) Transcript and protein fold changes for RNA binding and DNA repair proteins. Two-sample Wilcoxon test. H and I) Examples of proteins with negative (H) and positive (I) decoupling (N=3-4 biological replicates, MANOVA test). *P ≤ 0.05; **P ≤ 0.01, ***P ≤ 0.001, ****P ≤ 0.0001. Related to Fig. S1 and Table S1.

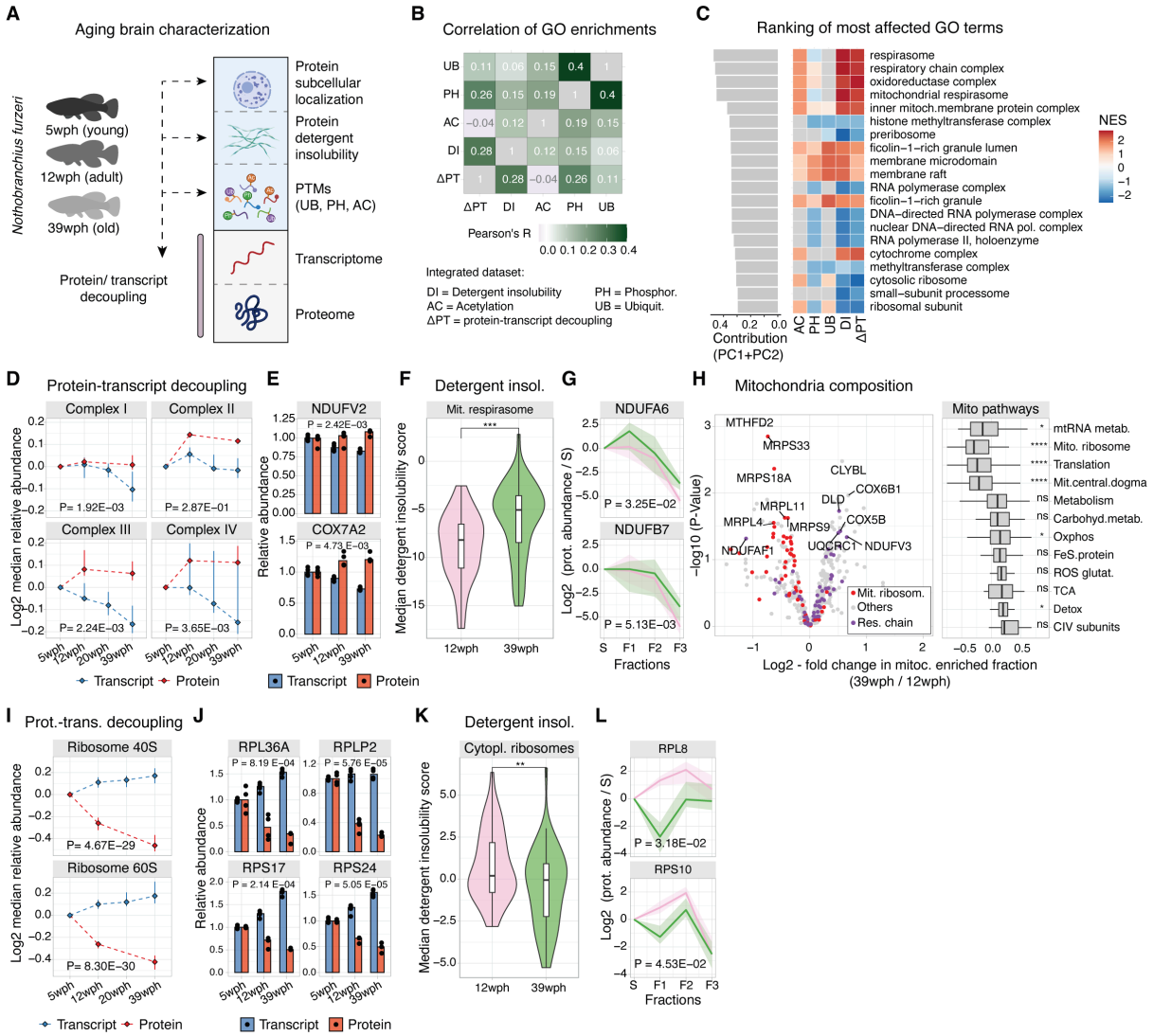

Figure 2: Age-related proteome changes converge on ribosomes and respiratory chain complexes. A) Overview of the datasets generated in this study (wph=weeks post-hatching). B) Heatmap showing correlations of normalized enrichment scores (NES) across datasets (DR=detergent insolubility, ΔPT=protein-transcript decoupling, AC=acetylation, PH=phosphorylation, UB=ubiquitylation). C) Top-ranking GO terms with strong contributions to PCA analysis. D) Line plots for respiratory chain proteins' transcript (blue) and protein (red) median abundance across age groups. Each point represents the median of the log2 ratio of the quantities relative to the young (5wph) age group. Vertical lines indicate 50% of the distribution (N=3-4 biological replicates, MANOVA test). E) Examples of respiratory chain proteins with positive protein-transcript decoupling (N=3-4 biological replicates, MANOVA test). F) Violin plot showing detergent insolubility scores of mitochondrial respirasome proteins (N=4 biological replicates, two-sample Wilcoxon test). G) Examples of detergent insolubility profiles for respiratory chain proteins with increased detergent insolubility during aging (N=4 biological replicates, MANOVA test). H) Volcano plot showing changes in mitochondrial proteome due to aging. The box plot shows the effect of aging on different groups of mitochondrial pathways (N=4 biological replicates, two-sample Wilcoxon test). I) Ribosomal proteins' transcript and protein abundance across age groups. Each point represents the median of the log2 ratio of the quantities relative to the young (5wph) age group. Vertical lines indicate 50% of the distribution (N=3-4 biological replicates, MANOVA test). J) Examples of ribosomal proteins displaying negative protein-transcript decoupling (N=3-4 biological replicates, MANOVA test). K) Violin plot showing detergent insolubility scores of cytoplasmic ribosomal subunits (N=4 biological replicates, two-sample Wilcoxon test). L) Examples of detergent insolubility profiles for ribosomal proteins with decreased detergent insolubility during aging (N=4 biological replicates, MANOVA test). *P ≤ 0.05; **P ≤ 0.01, ***P ≤ 0.001, ****P ≤ 0.0001. Related to Fig. S3 through S8 and Table S1, S4 and S5.

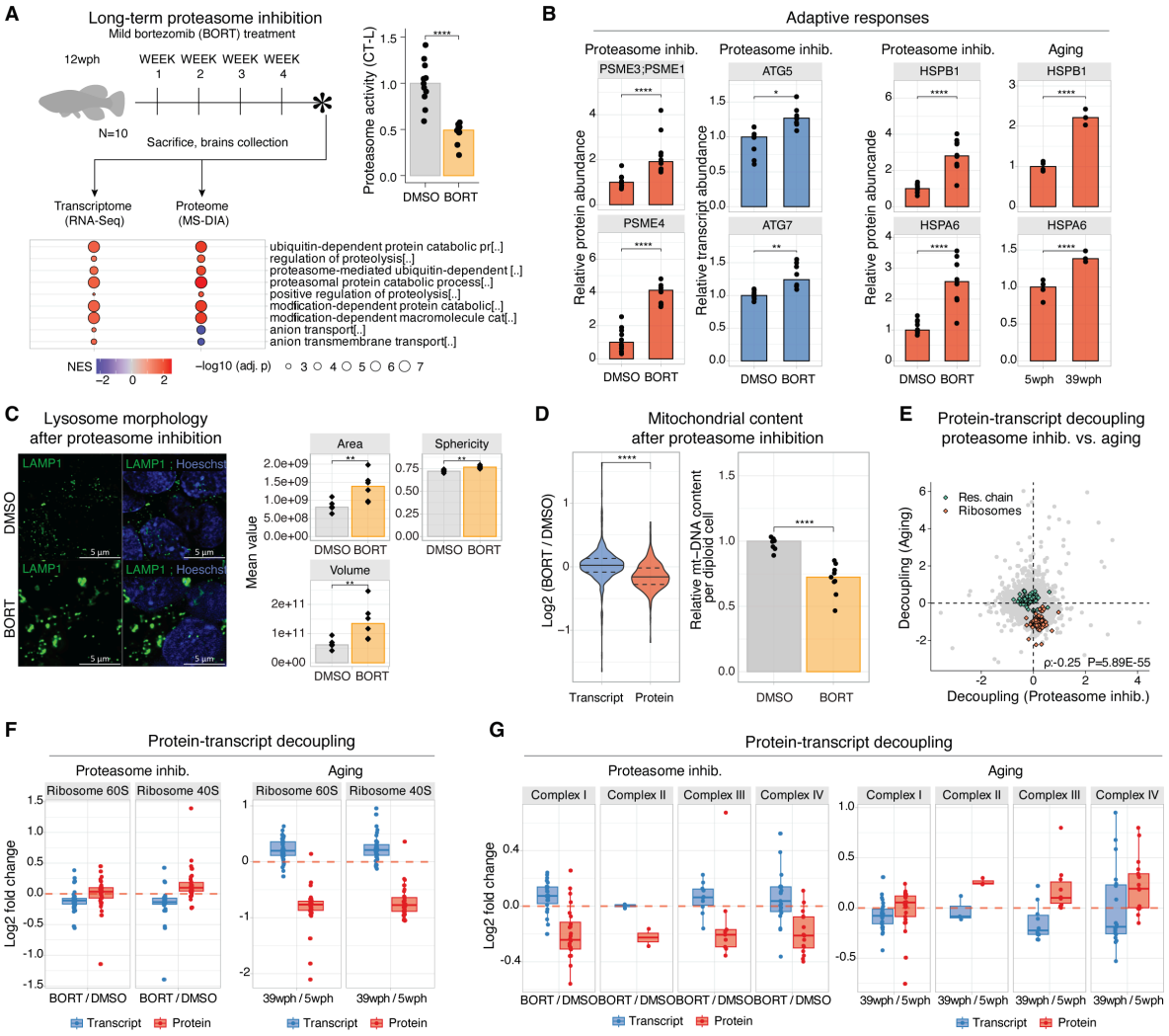

Figure 3: Effects of four weeks *in vivo* proteasome inhibition on the adult killifish brain. A) Adult killifish (12wph) received weekly intraperitoneal injections of the proteasome inhibitor bortezomib or DMSO as vehicle control. Bottom panel: gene Set Enrichment Analysis (GSEA) color-coded by normalized enrichment score (NES). Top-right: chymotrypsin-like proteasome activity quantification (N=10 biological replicates, two-sample Wilcoxon test). B) Barplot showing protein (red) and transcript (blue) abundance changes of selected proteins involved in proteostasis during aging and following proteasome inhibition. Asterisks indicate Q-values from Spectronaut for proteins and Adj. P-values from DESeq2 for transcripts (N=10 biological replicates). C) Effect of proteasome inhibition on lysosome morphology based on lysosome-associated membrane protein 1 (LAMP1) immunofluorescence (left, scale bars = 5µm) and quantification (right, N=6 biological replicates, two-sample t-test). D) Effect of proteasome inhibition on mitochondrial transcripts and proteins (left, two-sample Wilcoxon test) and mtDNA (right, N=10 biological replicates, two-sample Wilcoxon test). mtDNA copy number was calculated using real-time quantitative PCR with primers for 16S rRNA mitochondrial gene and cyclin-dependent kinase inhibitor 2a/b (Cdkn2a/b) nuclear gene for normalization. E) Comparison of decoupling scores between aging and proteasome inhibition. Respiratory chain and ribosomal proteins are highlighted in green and orange, respectively. Spearman correlation was chosen due to the presence of outliers in the distribution. F and G) Boxplot showing decoupling scores for ribosomal (F) and respiratory chain (G) proteins during aging and following proteasome inhibition. *P≤0.05; **P≤0.01, ***P≤0.001, ****P≤0.0001. Related to Fig. S9, Table S7.

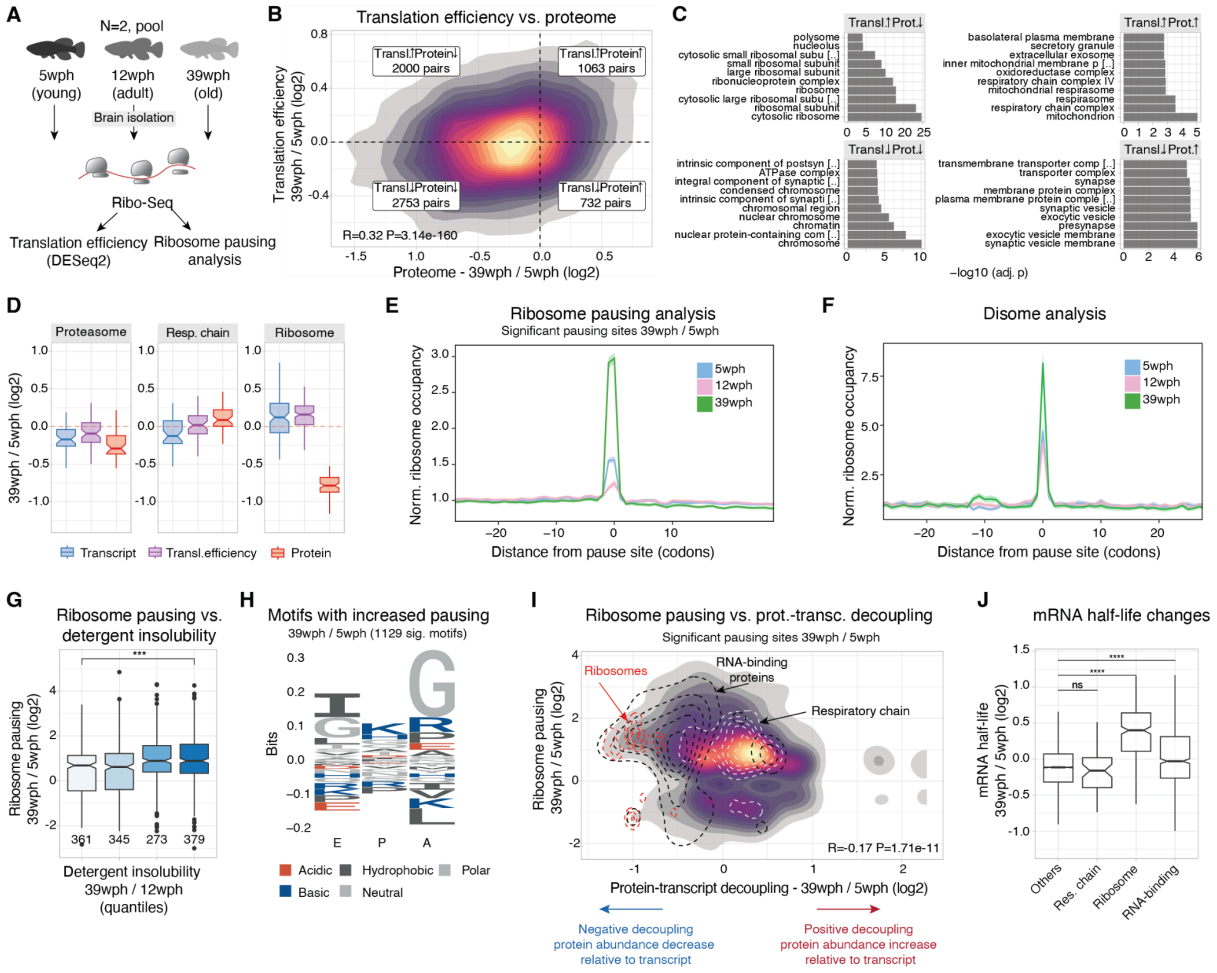

Figure 4: Increased translation pausing in the aging brain. A) Ribosome profiling was conducted on brains of killifish of different ages. Each age group had two replicates consisting of independent pooled samples from 10-15 animals. B) 2-D density plot comparing age-related changes in protein abundance (x-axis) and alterations in translation efficiency (y-axis). Different quadrants highlight distinct modalities of translation regulation. C) GO enrichment over-representation analysis for each quadrant of panel B (Fisher test with Holm correction). D) Boxplots comparing age-related changes of mRNA abundance (blue), translation efficiency (purple) and protein abundance (red) for 26S proteasome, respiratory chain complexes, and cytoplasmic ribosomes. E) Line plot showing the normalized ribosome distribution at pausing sites across different age groups. F) Line plot depticing normalized disome ribosome distribution at disome pausing sites for various age groups. G) Boxplot comparing ribosome pausing and age-related changes of protein solubility. Proteins encoded by transcripts displaying significant ribosome pausing in the old vs. young comparison (Adj. P-value < 0.05) are grouped according to their age-related changes in detergent insolubility. The number of proteins in each quantile is indicated (two-sample Wilcoxon test). H) Logo plot of amino acids being decoded at age-dependent increased pausing sites (Pause score at 39wph > Pause score at 5wph and 12wph, and Pause score at 39wph > 6). E: tRNA exit site; P: peptidyl-tRNA binding site; A: aminoacyl-tRNA binding site. I) 2-D density plot showing the relation between significant pausing changes (Adj. P-value < 0.05) and decoupling. Contours: cytoplasmic ribosomes (red), RNA-binding proteins (black), oxidative phosphorylation (white). J) Boxplot showing estimated mRNA half-life changes with age for selected gene sets (two-sample Wilcoxon test with Holm correction). *P ≤ 0.05; **P ≤ 0.01, ***P ≤ 0.001, ****P ≤ 0.0001. Related to Fig. S10 and 11, Table S9.

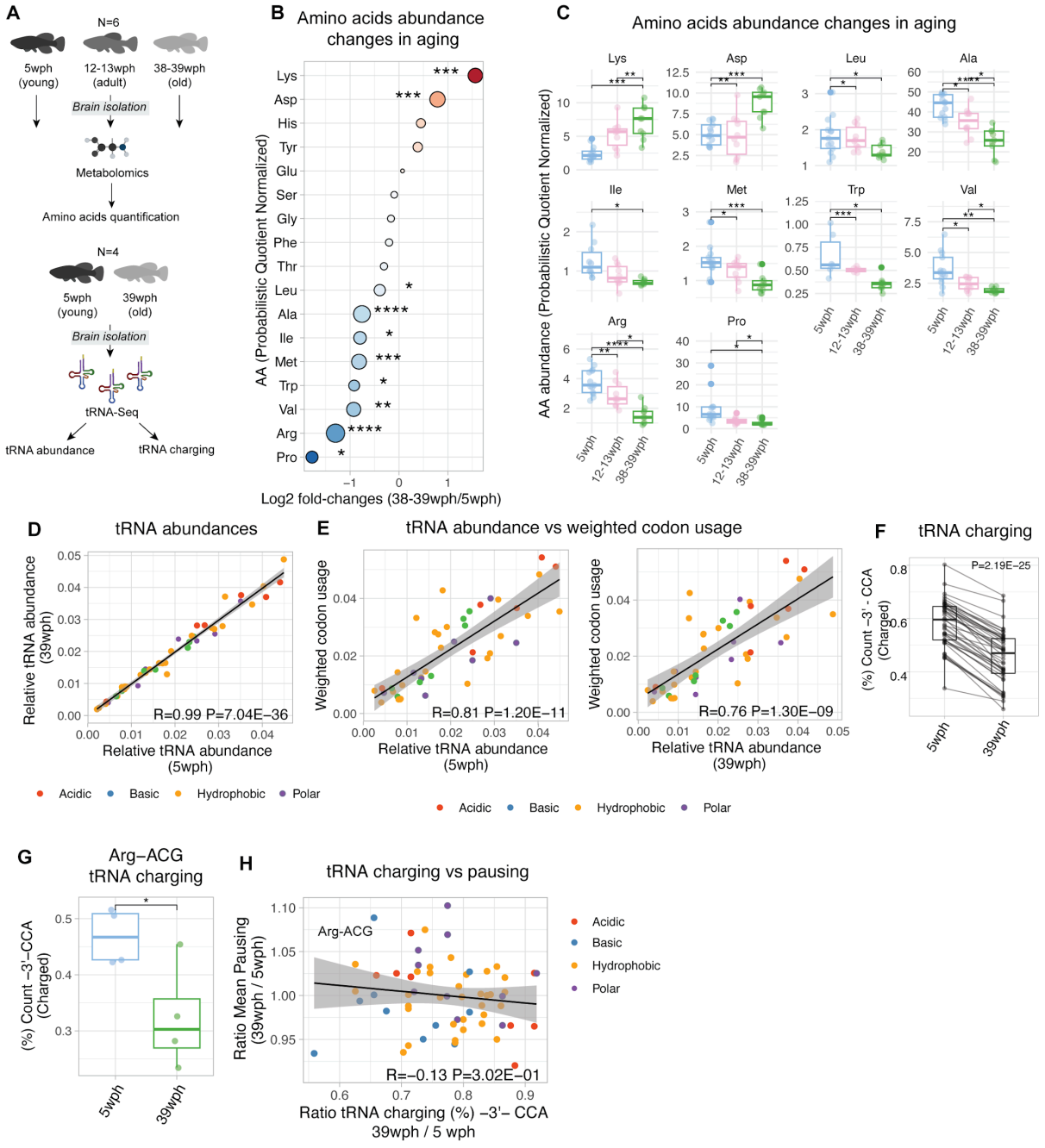

Figure 5: Changes of amino acid abundance and t-RNA charging in the aging brain

A) Metabolomics and tRNA-Seq were as conducted on brains of killifish of different ages. B) Dot plot showing changes of amino acid abundance in the aging killifish brain (N=6 biological replicates, two-sample t-test with Welch's correction). C) Boxplot displaying the quantification of amino acids that show significant (P-value<=0.05) age-related changes (N=6 biological replicates, two-sample t-test with Welch's correction). Amino acid abundances were obtained using tandem mass spectrometry (MS^2) and samples were normalized via probabilistic quotient normalization. D) Scatter plot comparing relative tRNA abundances and weighted codon usage (codon frequency normalized by transcript abundance) in young (left panel) and old (right panel) fish. Dots are colored according to the different amino-acid types that the tRNAs encode. E) Scatter plot showing the difference in relative abundance levels of tRNAs in young and old killifish. F) Boxplot showing the percentage of 3'-CCA counts for each tRNA, indicating the percentage of charged tRNAs in each sample (N=4 biological replicates, paired t-test). G) Boxplot showing changes in charging for the tRNA Arg-ACG (N=4 biological replicates, two-sample t-test with Welch's correction). H) Scatterplot showing the correlation between age-dependent changes in average pausing at each codon and changes in tRNA charging for the corresponding anticodon.n. Dots are colored according to the different amino-acid types that the tRNAs encode. *P ≤ 0.05; **P ≤ 0.01, ***P ≤ 0.001, ****P ≤ 0.0001. Related to Fig. S12, Table S10 and S11.

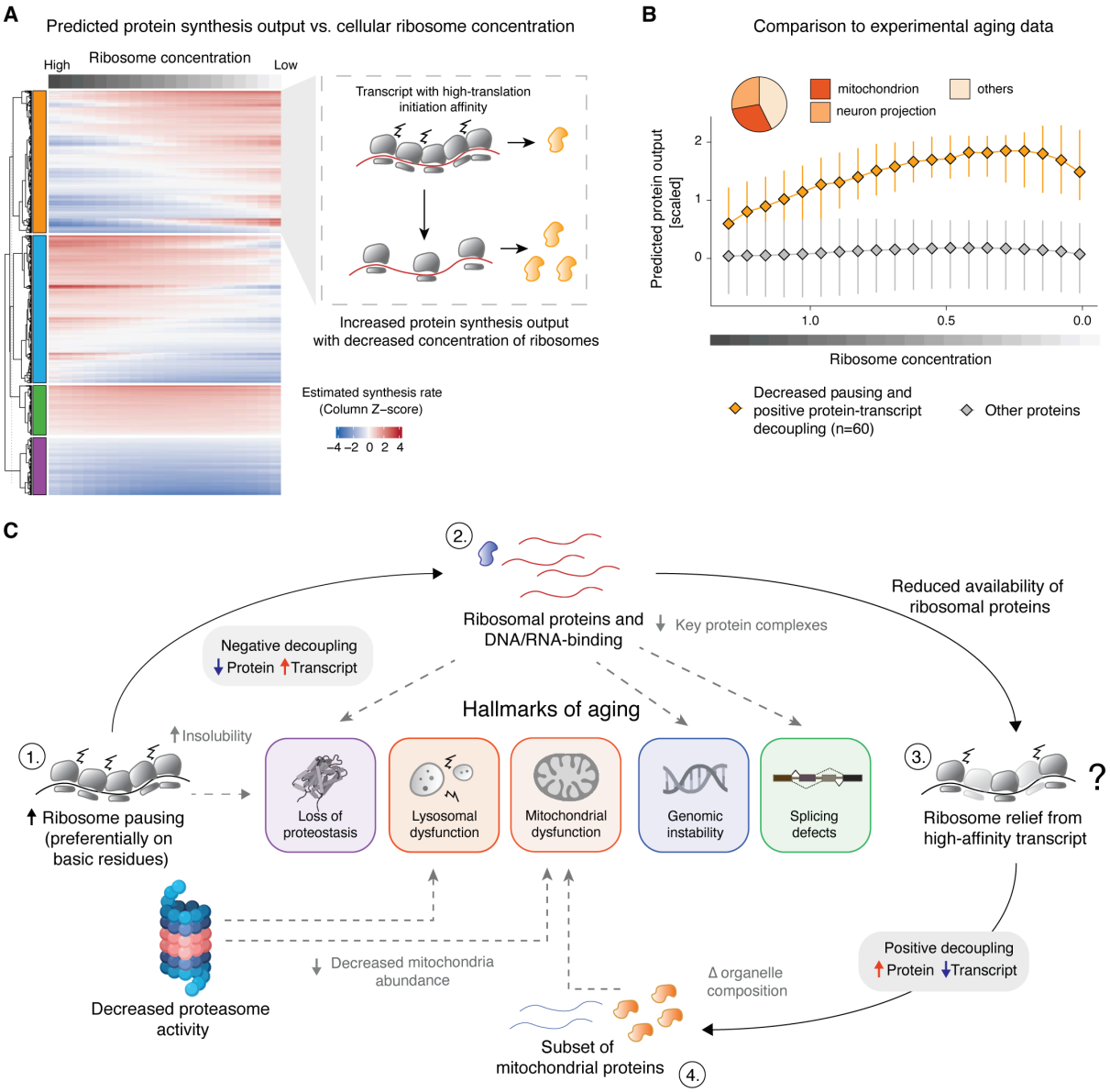

Figure 6: Decreased abundance of ribosomal proteins might lead to translation changes in the aging brain. A) Heatmap showing the estimated output of protein synthesis in relation to changes of ribosome concentration, modeled as described in Mills and Green 2017 (*42*, *43*). Columns indicate the estimated protein output for a specific ribosome concentration. Transcripts (rows) are clustered with a hierarchical clustering using the "ward D2" algorithm on the dissimilarity (1 - Person's correlation) measure. For display purposes, the heatmap shows 5000 randomly sampled transcripts. The right panel shows an illustrative example of a cluster displaying increased estimated protein output as a function of reduced ribosome abundance levels. For these transcripts, an overall decrease of ribosome concentration is predicted to reduce ribosome collisions and pausing on the mRNA, leading to overall increased protein synthesis output. B) Line plot showing the estimated protein synthesis output for transcript displaying decreased ribosome pausing in the killifish brain Ribo-Seq data (median per transcript log2 Pausing 39wph vs. 5wph < 0 and Adj. P-value <= 0.15) and positive decoupling with aging (increased protein abundance levels relative to the transcript, orange). The x-axis represents the simulated decreased ribosomal concentration, while the y-axis indicates the estimated protein output, as shown also in A. C) Schematic representation of the contribution of altered translation elongation and proteasome inhibition to other hallmarks of aging. An increase in translation elongation pausing occurs during brain aging in killifish correlating with a reduced synthesis of a subset of proteins enriched in basic amino acids, including ribosomal proteins. The decreased availability of ribosomal proteins and the ensuing reduction of translating ribosomes might favor the translation of mRNAs with high-translation initiation affinity, e.g., a subset of respiratory chain components, leading to increased abundance of the corresponding proteins in the aging brain. Proteasome inhibition affected aging hallmarks distinct from those linked to translation dysfunction and primarily impacted lysosome morphology and mitochondrial abundance. Related to Fig. S13, Table S12.